Scripta Materialia 146 (2018) 18–21

Contents lists available at ScienceDirect

Scripta Materialia

journal homepage: www.elsevier.com/locate/scriptamat

Regular article

Phase separation and zero thermal expansion in antiperovskite $Mn_3Zn_{0.77}Mn_{0.19}N_{0.94}$: An *in situ* neutron diffraction investigation

Sihao Deng [a,b], Ying Sun [a,*], Hui Wu [c], Zaixing Shi [a], Lei Wang [a], Jun Yan [a], Kewen Shi [a], Pengwei Hu [a], Xungang Diao [a], Qingzhen Huang [c], Christoph Sürgers [d], Cong Wang [a,*]

[a] Center for Condensed Matter and Materials Physics, Department of Physics, Beihang University, Beijing 100191, People's Republic of China
[b] Fundamental Science on Nuclear Wastes and Environmental Safety Laboratory, Southwest University of Science and Technology, Mianyang 621010, People's Republic of China
[c] NIST Center for Neutron Research, National Institute of Standards and Technology, Gaithersburg, MD 20899-6102, USA
[d] Physikalisches Institut, Karlsruhe Institute of Technology, P.O Box 6980, Karlsruhe 76049, Germany

ARTICLE INFO

Article history:
Received 11 September 2017
Received in revised form 18 October 2017
Accepted 27 October 2017
Available online xxxx

Keywords:
Antiperovskite compounds
Phase separation
Zero thermal expansion
Neutron diffraction

ABSTRACT

The antiperovskite $Mn_3Zn_{0.77}Mn_{0.19}N_{0.94}$ was investigated by *in situ* neutron powder diffraction (NPD) in the temperature region 5–300 K. Here, a noncollinear-antiferromagnetic/collinear-ferrimagnetic phase separation (PS) showing different lattice parameters was firstly revealed in antiperovskites. The NPD results prove that the noncollinear antiferromagnetic phase, even coexisting with the collinear ferrimagnetic phase, could be responsible for the zero thermal expansion behavior of $Mn_3Zn_{0.77}Mn_{0.19}N_{0.94}$ below 110 K. These findings suggest that Mn_3ZnN based materials could open a new avenue for further exploring the noncollinear magnetic PS and correlated physical properties of antiperovskites.

Noncollinear triangular antiferromagnets with Γ^{5g} symmetry and antiperovskite crystal structure recently gained significant attention due to their interesting physical properties, such as giant barocaloric [1], baromagnetic [2], piezomagnetic effects [3], as well as negative thermal expansion (NTE) [4–7] and zero thermal expansion (ZTE) [8–11]. So far, many efforts have been made on antiperovskite Mn_3AN (A = Cu, Zn, *etc.*) compounds for tuning the related properties of the Γ^{5g} antiferromagnetic (AFM) phase [12], especially the ZTE caused by strong spin-lattice coupling of the Γ^{5g} AFM phase [9–10]. In Mn_3Zn_xN and $Mn_3[Zn-(Ag,Ge)]_xN$, the temperature range for nearly ZTE from well above room temperature to well below can be tuned by vacancy generation and chemical substitution [10]. In a recent study, the Γ^{5g} phase has been stabilized by substitution of Mn at the Ni site in $Mn_{3+x}Ni_{1-x}N$ compounds, leading to the observed ZTE behavior [13].

Mn-based antiperovskite compounds with a triangular magnetic lattice show a variety of magnetic structures, including collinear, noncollinear, and even noncoplanar ones [14–16]. This indicates that these materials could be a valuable candidate to explore the noncollinear magnetic phase separation (PS). PS in strongly correlated electronic materials has been a stimulating topic because of the accompanied presence of some fascinating phenomena, such as granular superconductivity in cuprates [17], relaxor response in dielectric compounds [18], colossal magnetoresistance in manganites [19], and resistive switching in antiperovskites [20]. Notably, the PS of noncollinear and collinear AFM phases was observed in Mn_3ZnN, which leads to a resistive-switching phenomenon [20]. Recently, driven by the magnetic phase transition of noncollinear antiferromagnetic/ferrimagnetic (AFM/FIM) phases, a large baromagnetic effect was found in $Mn_3Ga_{0.95}N_{0.94}$ [2]. PS in antiperovskite compounds could promote a multifaceted interaction between magnetic phases [21]. Hence, the exploration of this PS could pave the way toward the advance of physical properties in antiperovskite materials, such as a large entropy change triggered by the appearance of FM phase at the AFM transition under an external magnetic field [22], a larger baromagnetic effect compared to that in $Mn_3Ga_{0.95}N_{0.94}$ [2], *etc.*

One of the outstanding candidates for investigating the PS of antiperovskites with a Γ^{5g} AFM phase is Mn_3ZnN and its doped compounds. In Mn_3ZnN, the PS of two AFM phases was found in the temperature interval of 140–177 K [23]. The coexistence of Γ^{5g} AFM and PM around the AFM-PM magnetic transition was revealed in $Mn_3Zn_{0.5}Ge_{0.5}N$ and $Mn_3Zn_{0.83}Mn_{0.15}N_{0.99}$ [10,24]. It is known that Mn atoms at the corners of the crystallographic unit cell of Mn_3AN make an important contribution to the magnetic exchange interaction [25,26]. Therefore, Mn_3ZnN with the Mn dopants at the corner is an excellent candidate for the study of a possible PS behavior. In this study, we present the results of an *in situ* neutron powder diffraction (NPD) investigation as a function of temperature (5–300 K). The PS behavior, consisting of a large-lattice noncollinear Γ^{5g} AFM and a small-lattice collinear FIM phase, was found to appear below 120 K in

* Corresponding authors.
E-mail addresses: sunying@buaa.edu.cn (Y. Sun), congwang@buaa.edu.cn (C. Wang).

http://dx.doi.org/10.1016/j.scriptamat.2017.10.031
1359-6462/

$Mn_3Zn_{0.77}Mn_{0.19}N_{0.94}$ compound, supported by magnetization measurements. To our best knowledge, this is the first time to report the PS of noncollinear AFM/collinear FIM in antiperovskite compounds.

A polycrystalline sample with a nominal composition $Mn_3Zn_{0.75}N$ was prepared by solid-state reaction in vacuum (10^{-5} Pa) using fine powders of Mn_2N and Zn (3N) [24]. NPD data from this sample were collected *in situ* as a function of temperature (5–300 K) using the BT-1 high-resolution neutron powder diffractometer at the NIST Center for Neutron Research (Gaithersburg, USA). A Cu (311) monochromator with a wavelength of 1.5398 Å was used. The intensities were measured with a step of 0.05° in the 2θ range 4–162° to study the thermal evolution of crystal and magnetic structures. The crystal and magnetic structures were analyzed by the Rietveld refinement method with the General Structure Analysis System (GSAS) program, using neutron scattering amplitudes −0.373, 0.568, and 0.936 ($\times 10^{-12}$ cm) for Mn, Zn, and N, respectively [24,27]. The Rietveld refinement could be fitted well with a structure model of cubic symmetry which has space group *Pm*-3*m* (No. 221) and the following atomic positions: Mn: 3c (0, 1/2, 1/2); Zn/Mn_2: 1a (0, 0, 0); N: 1b (1/2, 1/2, 1/2) [10]. The temperature dependence of magnetization was measured between 10 and 255 K under the applied magnetic fields of 100 Oe using a Physical Property Measurement System (PPMS). The measurement was conducted under zero-field cooling. Isothermal magnetization curves were recorded between −40 and 40 kOe at 10 and 130 K. Differential scanning calorimetry (DSC) measurement was conducted using Netzsch thermal equipment from 107 K to 300 K.

First, we analyze the crystal structure of the sample. Fig. 1(a) shows the NPD patterns of the nominal composition $Mn_3Zn_{0.75}N$ at 300 K. The site occupancies of the atoms Mn: 3c, Zn/Mn_2: 1a and N: 1b were investigated in detail, and the refinement results indicated that the real composition of $Mn_3Zn_{0.75}N$ is deficient in the cubic corners and body-centered sites [24]. The refined composition is determined to $Mn_3Zn_{0.77}Mn_{0.19}N_{0.94}$, indicating that Zn substitution by Mn in fact occurs, in contrast to the nominal composition $Mn_3Zn_{0.75}N$ with 25% Zn vacancies. This is in agreement with the refined NPD data of $Mn_3Zn_{0.83}Mn_{0.15}N_{0.99}$ and $Mn_{3+x}Ni_{1-x}N$ [13,24]. A small amount of MnO could be detected as impurity in Fig. 1(a). The refined lattice constant of $Mn_3Zn_{0.77}Mn_{0.19}N_{0.94}$ is 3.89272(9) Å at 300 K. Moreover, we calculated the NPD data above 120 K using the cubic structure model, and the results revealed that the cubic lattice with space group *Pm*-3*m* is reasonable. However, at temperatures below 120 K, additional features such as peak splittings could be observed in the NPD patterns. To highlight these features clearly, Fig. 1(b) and (c) show the thermal evolutions of the (211) NPD nuclear peak and the selected magnetic peak, respectively. Upon cooling below 120 K the (211) nuclear peak splits into two peaks, and the magnetic peak intensity suddenly increases while with increasing temperature above 120 K, the magnetic peak intensity decreases rapidly until it almost vanishes above 200 K. These characteristics indicate that there is a close correlation between the nuclear peak splitting and the intensities of the magnetic peaks, implying a PS behavior in $Mn_3Zn_{0.77}Mn_{0.19}N_{0.94}$.

The magnetic behaviors of $Mn_3Zn_{0.77}Mn_{0.19}N_{0.94}$ are clearly shown in Fig. 2. Two distinct magnetic transitions are observed in the temperature dependence of M(T) and dM/dT at 112 K and 200 K, see Fig. 2(a). Moreover, from Fig. 2(b), it is seen that the M - H curves at 10 K and 130 K exhibit FM characteristic. However, the magnetization at 10 K and 130 K does not saturate even though the field is increased to 40 kOe, which is attributed to the coexistence of FM and AFM ordered phases. Additionally, as displayed in Fig. 2(a), a peak in measured differential scanning calorimetry curve is observed at 118 K signifying a first-order phase transition.

To understand the nuclear peak splitting, the NPD pattern of $Mn_3Zn_{0.77}Mn_{0.19}N_{0.94}$ measured at 120 K is analyzed as shown in Fig. 3(c). Rietveld analysis indicates that these features are neither due to a structural transition nor a symmetry change. The best fits to the observed NPD patterns are achieved by the two-phase model, where two

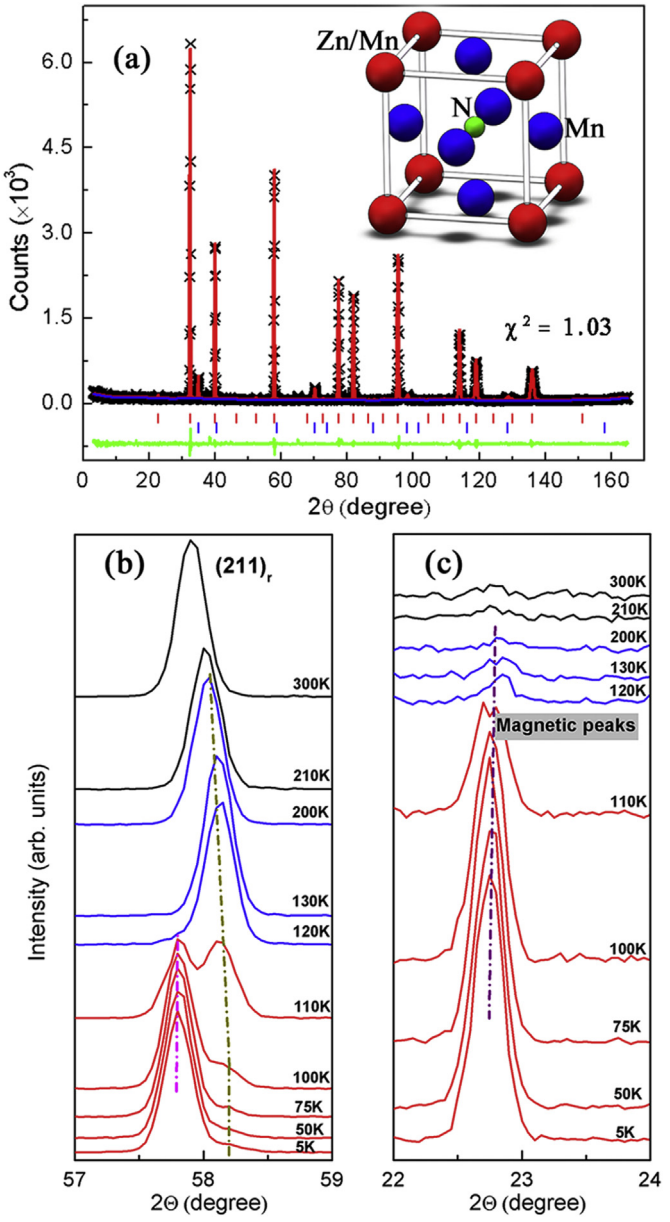

Fig. 1. (a) Neutron powder diffraction patterns of $Mn_3Zn_{0.77}Mn_{0.19}N_{0.94}$ at 300 K. The crosses show the experimental intensities (I_{obs}); the top solid line (red) shows the calculated intensities (I_{calc}), and the bottom solid line (green) is the difference between the observed and calculated intensities (I_{obs} - I_{calc}). The vertical lines indicate the angular positions of the nuclear peaks of $Mn_3Zn_{0.77}Mn_{0.19}N_{0.94}$ (red) and MnO (blue). The inset of (a) shows the crystal structure of $Mn_3Zn_{0.77}Mn_{0.19}N_{0.94}$, space group *Pm*-3*m* (No. 211), atomic positions Mn: 3c, Zn/Mn_2: 1a, N: 1b. Refined structural parameters of $Mn_3Zn_{0.77}Mn_{0.19}N_{0.94}$ are shown in Table S-I. Thermal evolutions of neutron powder diffraction (b) nuclear peak (211) and (c) magnetic peak of $Mn_3Zn_{0.77}Mn_{0.19}N_{0.94}$. (For interpretation of the references to color in this figure legend, the reader is referred to the web version of this article.)

cubic phases with the same space group coexist but have slightly different lattice parameters [10,23]. For the magnetic structure refinement, the magnetic peaks described by a rhombohedral (*R*-3) magnetic symmetry (Γ^{5g}AFM) belongs to the cubic phase with a larger volume [23], and the rest magnetic reflections can be better explained by a FIM model for the other phase with a smaller unit cell. Both models are shown in Fig. 3(a) and (b). A more detailed refinement for FIM model is proved in Fig. S-I. The refined lattice constants of these two phases are 3.9009(4) and 3.8796(1) Å, respectively. The refined moment in Γ^{5g} AFM phase is 2.5(4) μ_B/Mn and the components in FIM phase are 0.5(1) (face-centered atom) and 1.3(7) (corner atom) μ_B/Mn for Mn